Electronic supplementary information

Resonance-driven dynamically bipolar organic semiconductors for high-performance optoelectronic applications

He Jiang,[a] Ye Tao,[a] Jibiao Jin,[a] Yizhong Dai,[a] Lijie Xian,[a] Jun Wang,[a] Shuang Wang,[a] Runfeng Chen,*[a] Chao Zheng [a] and Wei Huang[a,b]

[a]Key Laboratory for Organic Electronics and Information Displays & Jiangsu Key Laboratory for Biosensors, Institute of Advanced Materials (IAM), Nanjing University of Posts & Telecommunications, 9 Wenyuan Road, Nanjing 210023, China.
[b]Frontiers Science Center for Flexible Electronics (FSCFE), Shaanxi Institute of Flexible Electronics (SIFE) & Shaanxi Institute of Biomedical Materials and Engineering (SIBME), Northwestern Polytechnical University (NPU), 127 West Youyi Road, Xi'an 710072, China.

Table of Contents

1. Materials and synthesis

Materials: All materials and reagents, unless otherwise specified, were purchased from commercial suppliers and used without further purification. The final products were subjected to vacuum sublimation to further improve purity before photoluminescence (PL) and electroluminescence (EL) measurements.

Structure characterization instruments: ^{1}H and ^{13}C-nuclear magnetic resonance (NMR) spectra were recorded on a Bruker Ultra Shield Plus 400 MHz instrument (400 MHz for ^{1}H and 100 MHz for ^{13}C, respectively) with dimethyl sulfoxide (DMSO)-d_6 or CDCl$_3$ as the solvents and tetramethylsilane (TMS, δ = 0.00 ppm) as the internal standards. The quoted chemical shifts are in *ppm* and the coupling constants (*J*) values are expressed in Hz. The splitting patterns have been designed as follows: s (singlet), d (doublet), t (triplet) and m (multiplet). High resolution mass spectra (HRMS) were recorded on a LCT Premier XE (Waters) HRMS spectrometry. Fourier transform infrared spectroscopy (FTIR) spectra were recorded with KBr pellet using Perkin Elmer Spectrum Two IR spectrometer.
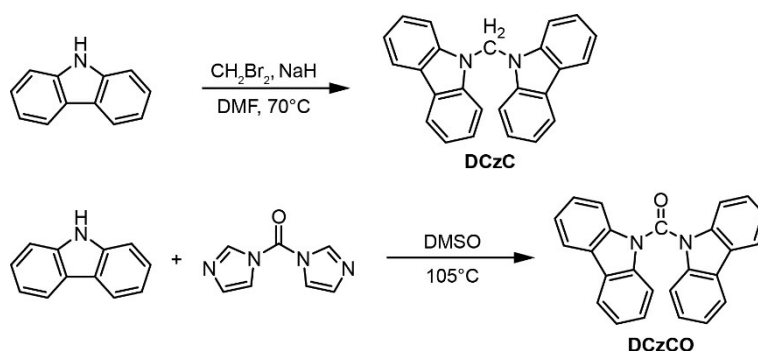
Scheme S1. Synthetic routes of **DCzC** and **DCzCO**.

Synthesis of di(9*H*-carbazol-9-yl)methane (DCzC):

A solution of carbazole (0.50 g, 2.99 mmol) and sodium hydride (NaH, 60% dispersion in mineral oil, 0.16 g, 6.48 mmol) in dehydrated *N*, *N*-dimethylformamide (DMF, 10 mL) was stirred at room temperature under nitrogen atmosphere for 1 h. Dibromomethane (CH$_2$Br$_2$,

0.11 mL, 1.50 mmol) was then added slowly to the above solution. The mixture was then heated at 70ºC for 6 h to complete the reaction. After cooling to the room temperature, the reaction solution was poured into water (100 mL) and the precipitated solids were collected by filtration and dissolved in dichloromethane (CH_2Cl_2, 100 mL). The organic solution was dried with anhydrous sodium sulphate (Na_2SO_4). The solvent of CH_2Cl_2 was removed under reduced pressure and the residue was purified with flash column chromatography over silica gel using petroleum ether (PE):CH_2Cl_2 (5:1, vol/vol) as eluent to afford the compound as white powder.[1] Yield: 81%. ^{1}H NMR (DMSO- d_6, 400 MHz) δ (ppm): 8.20 (d, J=8 Hz, 4H), 7.70 (d, J=8 Hz, 4H), 7.43 (t, J=16 Hz, 4H), 7.25 (t, J=16 Hz, 4H), 7.13 (s, 2H). ^{13}C NMR (CDCl$_3$, 100 MHz) δ (ppm): 140.12, 126.29, 123.72, 120.60, 120.08 109.31, 52.63. HRMS (EI): m/z calcd for $C_{25}H_{18}N_2$ [M+Na]$^+$: 369.1368; found: 369.1368.
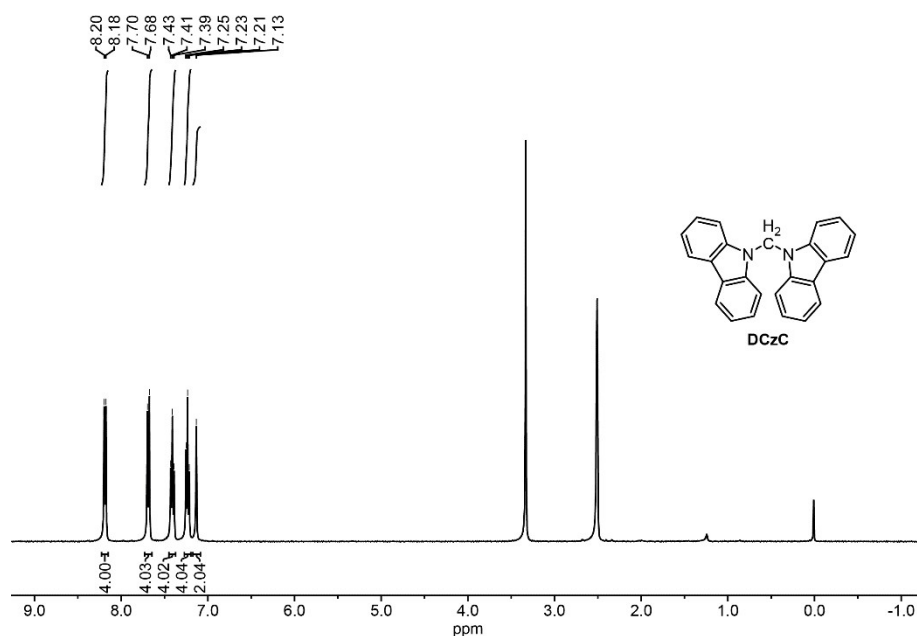
Figure S1. ^{1}H NMR spectrum of **DCzC** in DMSO- d_6.
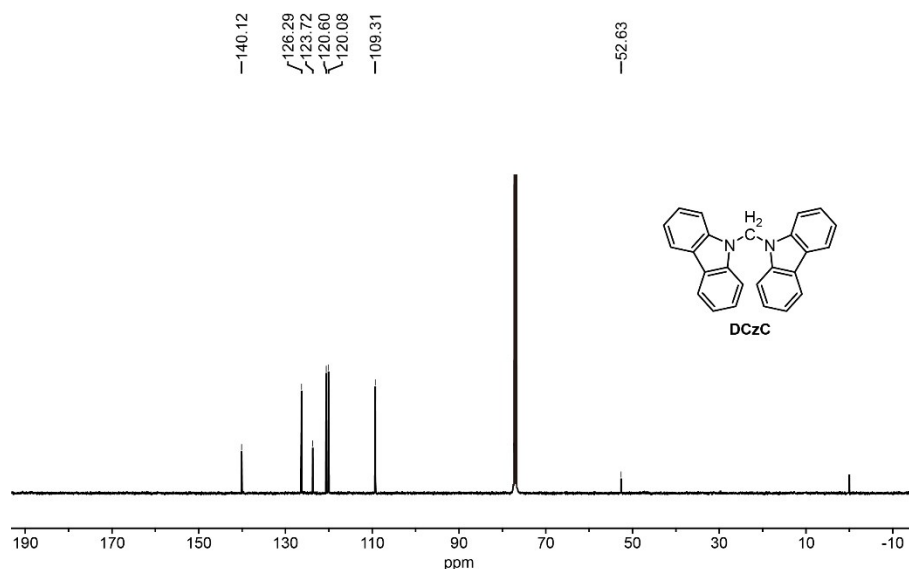
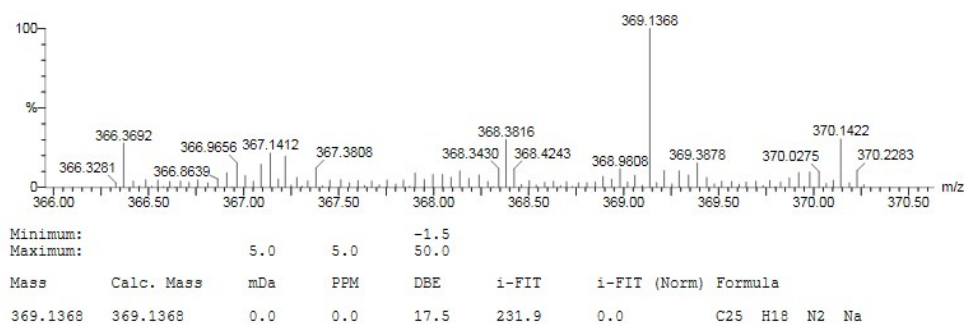**Figure S2.** ^{13}C NMR spectrum of **DCzC** in CDCl$_3$.

Figure S3. HRMS spectrum of **DCzC**.

Synthesis of di(9*H*-carbazol-9-yl)methanone (DCzCO):

A solution of carbazole (0.50 g, 2.99 mmol) and *N,N'*-carbonylimidazole (0.24 g, 1.50 mmol) in dehydrated DMSO (10 mL) was heated at 105℃ under nitrogen atmosphere for 6 h. After cooling to room temperature, the reaction solution was poured into water (100 mL) and the participate was collected and dissolved in CH$_2$Cl$_2$ (100 mL). The CH$_2$Cl$_2$ solution was dried with anhydrous Na$_2$SO$_4$. By removing the solvent of CH$_2$Cl$_2$ under reduced pressure, the residue was purified with flash column chromatography over silica gel using PE:CH$_2$Cl$_2$ (5:1, vol/vol) as eluent to afford the compound as white powder.[2] Yield: 44%. ^{1}H NMR (DMSO-d_6, 400 MHz) δ (ppm): 8.30 (d, *J*=8 Hz, 4H), 7.44-7.37 (m, 8H), 7.43 (d, *J*=8 Hz, 4H). ^{13}C

NMR (CDCl$_3$, 100 MHz) δ (ppm): 149.53, 137.95, 127.24, 125.91, 123.57 120.20, 114.58.

HRMS (EI): m/z calcd for C$_{25}$H$_{16}$N$_2$O [M]$^+$: 361.1347; found: 361.1341.
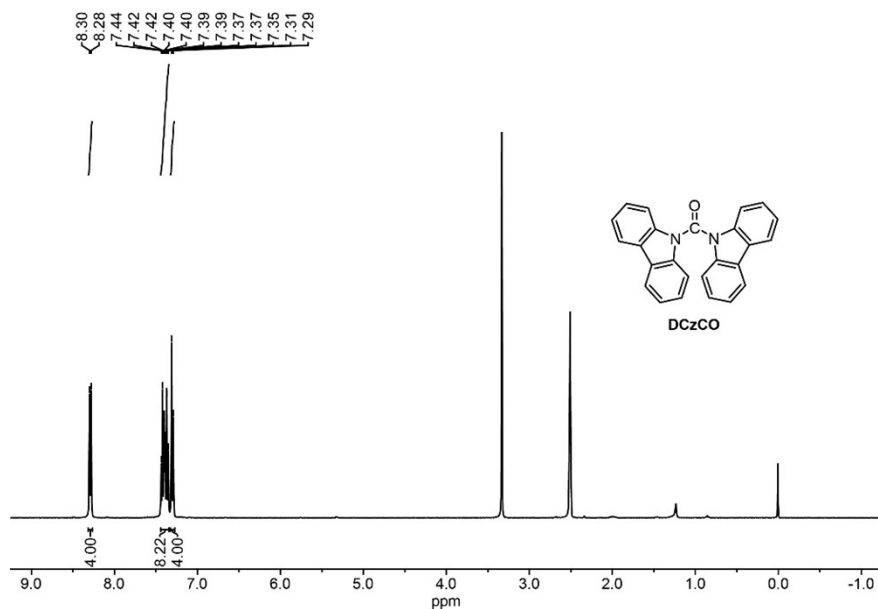
Figure S4. ^{1}H NMR spectrum of **DCzCO** in DMSO- d_6.
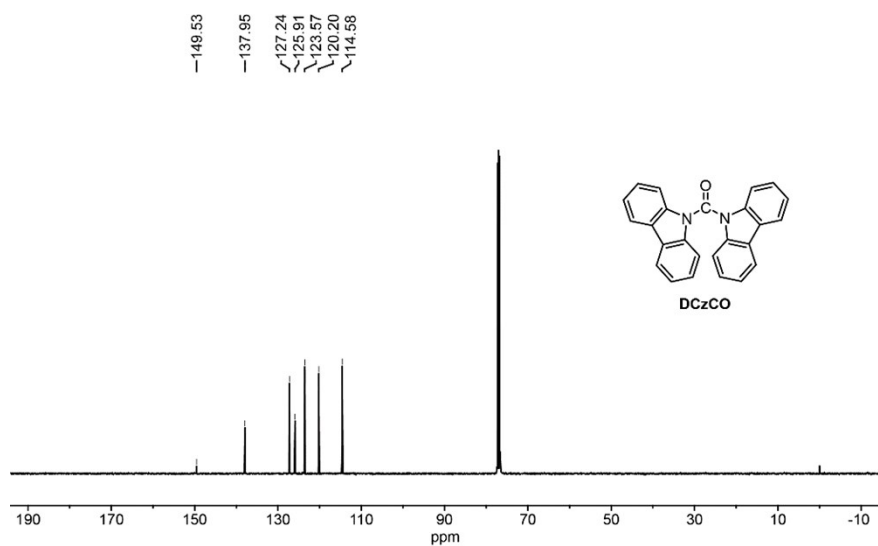

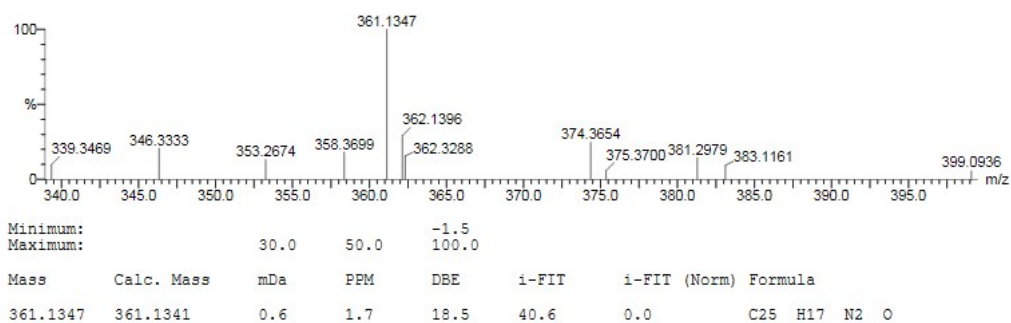**Figure S5.** ^{13}C NMR spectrum of **DCzCO** in CDCl$_3$.
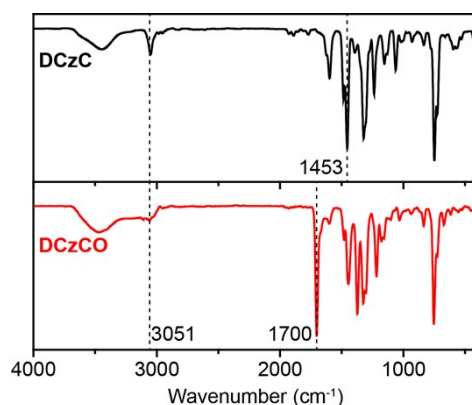
Figure S6. HRMS spectrum of **DCzCO**.

Figure S7. FTIR spectra of **DCzC** and **DCzCO**. Characteristic FTIR absorptions at 3051, 1700, and 1453 cm^{-1} correspond to stretching vibrations of aryl C-H and C=O bonds and CH$_2$ bending vibration, respectively.

2. Single crystal X-ray analysis

Single crystals of **DCzC** and **DCzCO** were grown by slow evaporation of a combined CH$_2$Cl$_2$ and ethanol solution at room temperature. Data of single crystal structures were collected at 296 K on a Bruker SMART APEX (II)-CCD area detector diffractometer with graphite-monochromated Mo-K_α radiation (λ = 0.71073 Å) in ω scan mode. All structures were solved by direct methods using the Olex2 1.2 programs and refined by full-matrix least-square techniques on F^2. All non-hydrogen atoms were refined anisotropically and the hydrogen atoms were added in idealized position and refined with isotropic displacement. The crystal structures were analyzed by Diamond 3.2 software. The CCDC numbers for **DCzC** and **DCzCO** are 1970706 and 1970715, respectively. The crystallographic data of their single crystal structures were summarized in **Table S1**. The crystallographic information files (CIF) were also attached.

6

**Table S1**. Crystallographic data of **DCzC** and **DCzCO** single crystals.

Compound	DCzC	DCzCO
Empirical formula	$C_{25}H_{18}N_2$	$C_{25}H_{16}N_2O$
Formula weight (g mol^{-1})	346.43	360.40
Crystal color	colorless	colorless
Wavelength (Å)	0.71073	0.71073
Crystal system	Monoclinic	Monoclinic
Space group	P 21/n	P 21/c
a (Å)	4.9504(7)	16.125(12)
b (Å)	18.053(2)	5.437(4)
c (Å)	19.902(3)	22.259(17)
α (deg)	90	90
β (deg)	92.566(3)	110.185(15)
γ (deg)	90	90
V (Å^3)	1776.9(4)	1832(2)
Z	4	4
Density (g cm^{-3})	1.295	1.307
μ (mm^{-1})	0.076	0.081
T_{min}, T_{max}	0.989,0.991	0.508,0.746
$F(000)$	728.0	752.0
h_{max}, k_{max}, l_{max}	6,24,26	21,7,29
$Theta_{max}$	28.552	28.106
CCDC Number	1970706	1970715

3. Thermal stabilities and film-forming properties

Solubility tests were made in tetrahydrofuran (THF), toluene, CH_2Cl_2, and trichloromethane (CHCl$_3$) at room temperature. Thermal properties of **DCzC** and **DCzCO** were investigated by thermogravimetric analysis (TGA) and differential scanning calorimetry (DSC). TGA measurements were conducted on a DTG-60 Shimadzu thermal analyst system under a heating rate of 10°C /min and a nitrogen flow rate of 50 cm^3/min. Temperature at 5% weight loss was used as the decomposition temperature (T_d). DSC analyses were performed on a Shimadzu DSC-60A instrument under a heating rate of 10°C /min and a nitrogen flow rate of 20 cm^3/min. The glass transition temperature (T_g) were determined from the first heating scan. As shown in Figure S8, both materials show good thermal stability with T_d of 297 and 257°C for **DCzC** and **DCzCO**, respectively. Meanwhile, **DCzC** show glass transition process with T_g of 111°C.

Table S2. Solubility tests of **DCzC** and **DCzCO** in mg mL^{-1}.

Compound	THF	Toluene	CH$_2$Cl$_2$	CHCl$_3$
DCzC	15	7	5	8
DCzCO	40	19	31	43
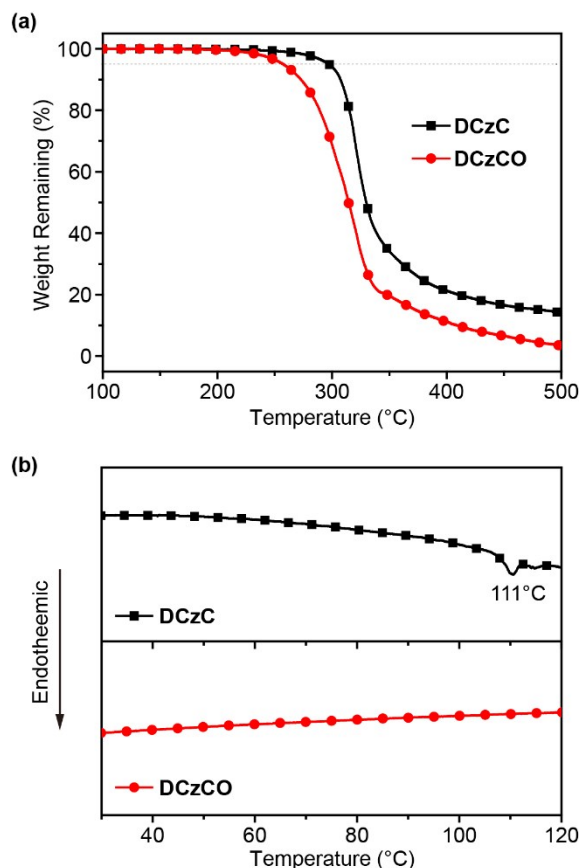
Figure S8. (a) TGA and (b) DSC curves of **DCzC** and **DCzCO**.

Atomic force microscopy (AFM) was carried out at room temperature to investigate the film-forming properties using a FSM-Precision FM-Nanoview 1000 AFM equipped with a Scanasyst-Air peak force tapping mode AFM tips from Bruker. Vacuum-evaporated thin films for AFM measurements were prepared on indium tin oxides (ITO)/ poly(3,4-ethylenedioxythiophene): poly(styrenesulfonate) (PEDOT:PSS) substrates. Uniform films of **DCzC** and **DCzCO** on ITO/PEDOT: PSS surfaces were identified by AFM images with low root mean square (RMS) roughness of 0.466 and 0.370 nm, respectively.
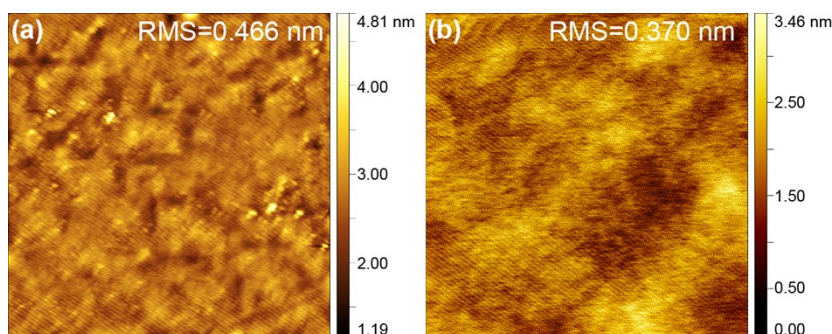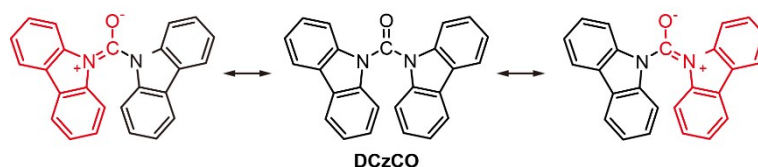
Figure S9. AFM images of the vacuum-evaporated thin films of (a) **DCzC** and (b) **DCzCO** on ITO/PEDOT: PSS substrates.

4. Main resonance structures

The facile resonance interconversion of **DCzCO** results in a large number of enantiotropic structures between neutral N-C=O and two polarized N^+=C-O^- canonical forms. The main resonance structures were illustrated in **Scheme S2**.

Scheme S2. Main resonance structures of **DCzCO**.

5. Computational details

Density functional theoretical (DFT) calculations were performed on Gaussian 09 program package.[3] The geometries of **DCzC** and **DCzCO** were firstly optimized by the widely used Beckes three-parameter exchange functional along with the Lee Yang Parr's correlation functional (B3LYP) at 6–31G(d) basis set. Comparing to the single crystal structures, better predictions were found using M06-2X with a large basis set of cc-pVTZ to consider the long range interactions. Therefore, M06-2X/cc-pVTZ was adopted to optimize not only the ground state (S_0) geometries but also the lowest triplet-state (T_1) geometries.[4] The frontier molecular orbital distributions and spin density distributions were predicted by M06-2X/cc-pVTZ based

9

on the optimized S_0 and T_1 geometries, respectively. The highest occupied molecular orbital (HOMO) and lowest unoccupied molecular orbital (LUMO) energy levels were calculated based on the S_0 geometries at B3LYP/6-31G(d) level. The T_1 energies were obtained by using the combination of TD-M06-2X/cc-pVTZ. Fuzzy bond order analysis embedded in Multiwfn was used to study the bond order of the resonance structures based on the single crystal structures.[5] NBO 6.0 program was used to perform Natural bond orbital (NBO) energetic analysis with HF/6-31G(d) method based on the single crystal structures. The energy of the resonance variation (E_{RV}) was estimated using the energy difference of idealized natural Lewis structure of N-C=O and N^+-C=O^- by deleting all Fock matrix elements between Lewis NBOs and the germinal non-Lewis NBOs.[6] The reduced density gradient (RDG) isosurface calculations were performed using Multiwfn version 3.3 software based on the dimer structures from the single crystal structures.

Reorganization energies of hole (λ_h) and electron (λ_e) were calculated by using ωB97x method based on the incoherent hopping model. This model assumes a charge transport process between two adjacent molecules $M^{\pm} + M \rightarrow M + M^{\pm}$, where M is the neutral molecule interacting with the neighboring cationic (M^-) or anionic molecule (M^+) to transfer the charge between them. Theoretically, λ_h and λ_e can be calculated by the following equations:

$$\lambda_h = \lambda_+ + \lambda_1 \qquad (S1)$$

$$\lambda_e = \lambda_- + \lambda_2 \qquad (S2)$$

$$\lambda_+ = E^+(M) - E^+(M^+) \qquad (S3)$$

$$\lambda_1 = E(M^+) - E(M) \qquad (S4)$$

$$\lambda_- = E^-(M) - E^-(M^-) \qquad (S5)$$

$$\lambda_2 = E(M^-) - E(M) \qquad (S6)$$

where $\lambda_{\pm}$ are the relaxation energy of a neutral molecule (M) that captured a hole or electron going toward the optimum geometry on the potential energy surface of cation (M^+) or anion

(M$^-$); λ_1 and λ_2 are the relaxation energy from M$^+$ or M$^-$ extracting a hole or electron going toward the M optimum geometry on the potential energy surface of M; E^+(M) and E^+(M$^+$) are the total energies of the cation species under the optimum geometry of M and M$^+$, respectively; E(M) and E(M$^+$) represent the total energies of the neutral molecule under the optimum geometry of M and M$^+$, respectively; E^-(M) and E^-(M$^-$) are the total energies of the anionic species under the optimum geometry of M and M$^-$, respectively.

Table S3. Fuzzy bond order analysis of **DCzC** and **DCzCO**.

Compound	Bond order	
	N-C	C=O
DCzC	1.108/1.108	-
DCzCO	1.164/1.127	1.973

Bond lengths and charge distributions

NBO analysis was performed to study the charge distribution of **DCzC** and **DCzCO** on the basis of optimized S$_0$ geometry predicted by M06-2X/cc-pVTZ. The distribution of the injected charge (δ_C) on the carbazole and methylene or carbonyl groups (CH$_2$ or CO) was calculated by **Equation S7-S9** by adding a negative (-1) charge on the molecule:

$$\text{Carbazole } (\delta_C) = \text{Carbazole } (-1) - \text{Carbazole } (0) \qquad (S7)$$

$$\text{CH}_2 \ (\delta_C) = \text{CH}_2 \ (-1) - \text{CH}_2 \ (0) \qquad (S8)$$

$$\text{CO } (\delta_C) = \text{CO } (-1) - \text{CO } (0) \qquad (S9)$$

Similarly, when a positive (+1) charge is injected, its distribution can be figured out by **Equation S10-S12**:

$$\text{Carbazole } (\delta_C) = \text{Carbazole } (+1) - \text{Carbazole } (0) \qquad (S10)$$

$$\text{CH}_2 \ (\delta_C) = \text{CH}_2 \ (+1) - \text{CH}_2 \ (0) \qquad (S11)$$

$$\text{CO } (\delta_C) = \text{CO } (+1) - \text{CO } (0) \qquad (S12)$$

Table S4. The selected bond lengths and charge distributions of **DCzC** and **DCzCO**.

Compound	Bond length (Å)[a]		Carbazole (δ_C)[b]		CH$_2$/C=O (δ_C)[b]	
	N-C	C=O	-1	+1	-1	+1
DCzC	1.444/1.445	-	-0.913/-0.069	0.486/0.486	-0.018	0.029
DCzCO	1.435/1.411	1.213	-0.252/-0.257	0.821/0.153	-0.491	0.026

[a]From experimental single crystal structures; [b]The charge distribution ratio (δ_C) on carbazoles and methylene or carbonyl groups (CH$_2$ or C=O) when adding electron (-1) or hole (+1) charge based on the optimized S$_0$ geometries.

Table S5. The energy of the resonance variation (E_{RV}) between N-C=O and N$^+$-C=O$^-$ resonance structures.

Compound	Structure	Energy (a.u.)	E_{RV} (eV)
	N$^+$=C-O$^-$	-1139.038929	0.399
DCzCO	N-C=O	-1139.053601	
	N$^+$=C-O$^-$	-1139.038997	0.397

Table S6. Electron cloud density distribution percentages of the frontier molecular orbitals for **DCzC** and **DCzCO**.

Compound	Carbazoles (%)						CH$_2$/C=O (%)					
	H$_{-2}$[a]	H$_{-1}$[a]	H[a]	L[a]	L$_{+1}$[a]	L$_{+2}$[a]	H$_{-2}$[a]	H$_{-1}$[a]	H[a]	L[a]	L$_{+1}$[a]	L$_{+2}$[a]
DCzC	48.85/ 48.71	49.85/ 50.10	48.91/ 49.08	49.88/ 49.49	49.40/ 49.79	49.94/ 49.91	2.45	0.05	2.01	0.63	0.81	0.15
DCzCO	46.58/ 49.03	51.14/ 48.74	49.27/ 49.38	50.07/ 49.89	38.93/ 39.20	40.34/ 40.22	4.38	0.12	1.34	0.04	21.87	19.44

[a]H, H$_{-1}$, H$_{-2}$ represent HOMO, HOMO$_{-1}$ and HOMO$_{-2}$; L, L$_{-1}$, L$_{-2}$ represent LUMO, LUMO$_{-1}$ and LUMO$_{-2}$, respectively.

6.   Photophysical properties

Ultraviolet-visible (UV-Vis) spectra were recorded on a JASCO V-750 spectrophotometer, while fluorescence spectra were obtained on an Edinburgh FLS980 fluorescence spectrophotometer with a Xenon lamp as light source. The phosphorescence spectra of the compounds in 2-Methyltetrahydrofuran (2-MeTHF) were measured using a time-resolved Edinburgh FLS980 fluorescence spectrophotometer at 77 K with a 10 ms delay time after the excitation (λ_{ex}=295 nm) using a microsecond flash lamp. Transient PL decay

curves were collected using an Edinburgh FLS 980 fluorescence spectrophotometer at room temperature under the excitation wavelength of 295 nm. The absolute photoluminescence quantum yield (PLQY) was obtained using an integrating sphere. The lifetimes of the luminescence were figured out by fitting the luminescent intensity decay curve (I(t)) with a multi-exponential decay function in **Equation S13**:

$$I(t) = \sum_i A_i e^{-\frac{t}{\tau_i}}$$ (S13)

where A_i and τ_i represent the amplitudes and lifetimes of the individual PL components in multi-exponential decay profiles, respectively. The energy transfer efficiency (η) from host to guest was calculated based on the lifetimes of the host film with (τ_1) or without (τ_2) guest doping according to **Equation S14**:
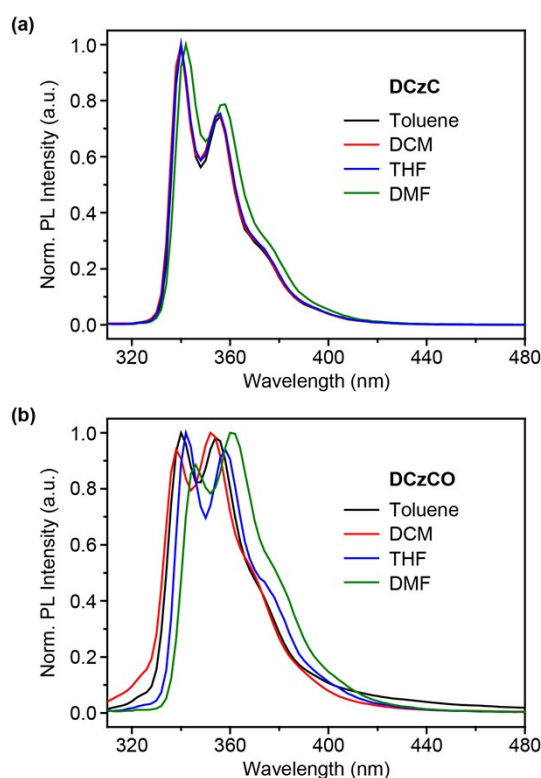
$$\eta = \frac{\tau_1 - \tau_2}{\tau_1}$$ (S14)

Figure S10. PL spectra of (a) **DCzC** and (b) **DCzCO** in different solvents with different polarities. The concentration of the emitters is ~10^{-5} mol L^{-1} and the excitation wavelength is at 295 nm.
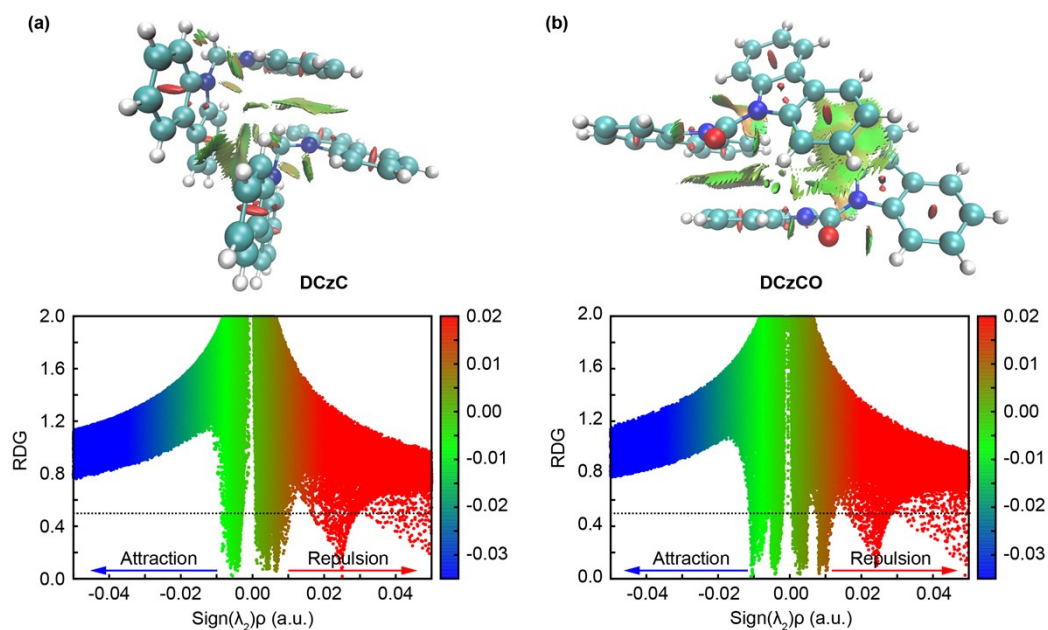
13

Figure S11. Reduced density gradient (RDG) versus sign(λ_2)ρ with the view of the RDG isosurface of (a) **DCzC** and (b) **DCzCO** dimers. Positive charges are in red, while negative charges are in blue.
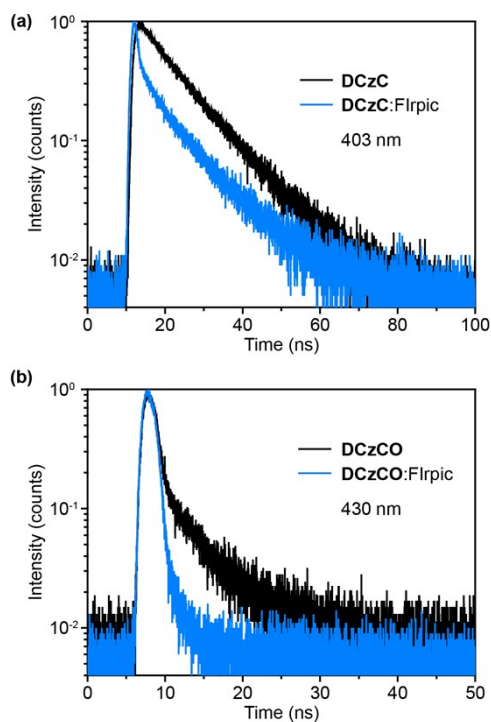

Figure S12. Transient PL decay curves of the excimer emission of (a) **DCzC** and (b) **DCzCO** films at 403 and 430 nm with (blue) or without (black) 18 wt% FIrpic doping. The excitation wavelength is at 295 nm.
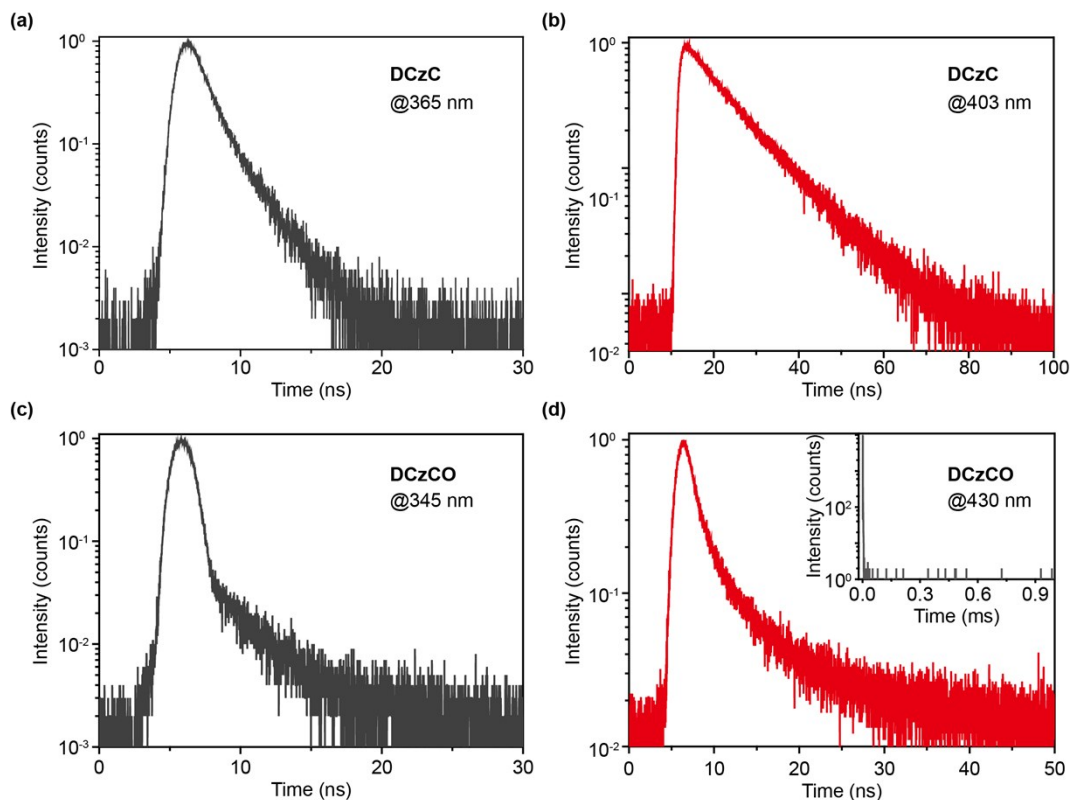
Figure S13. Transient PL decay curves of the 365 (a) and 403 nm (b) emission of **DCzC** film and the 345 (c) and 430 nm (d) emission of **DCzCO** film at room temperature under the excitation of 295 nm irradiation. Inset: transient PL decay curve of the 430 nm emission band of **DCzCO** film with a time range of 1 ms, where no long-lived phosphorescence was observed.
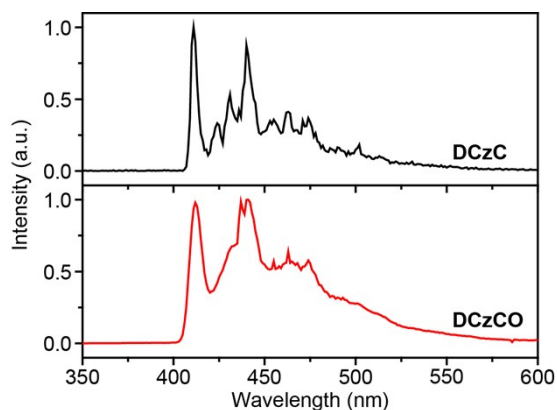

Figure S14. Phosphorescence spectra of **DCzC** and **DCzCO** in 2-MeTHF at 77 K with a delay of 10 ms after the 295 nm excitation.

7. Electrochemical properties

Cyclic voltammetry (CV) measurements were performed at room temperature on a CHI660E system in a typical three-electrode cell with a working electrode (glass carbon), a reference electrode (Ag/Ag$^+$, referenced against ferrocene/ferrocenium (FOC), and a counter electrode (Pt wire) in acetonitrile solution of tetrabutylammonium hexafluorophosphate (Bu$_4$NPF$_6$) (0.1 M) at a sweeping rate of 100 mV s^{-1}. HOMO energy levels (E_{HOMO}) of the materials were estimated based on the reference energy level of ferrocene (4.8 eV below the vacuum) according to **Equation S15**:

$$E_{HOMO} = - (E_{onset}^{Ox} - E_{(Fc/Fc^+)} + 4.8) \text{ eV} \qquad (S15)$$

where $E_{(Fc/Fc^+)}$ is the onset potential of oxidative wave of ferrocene (Fc) *vs* Ag/Ag$^+$ and E_{onset}^{Ox} is the onset potential of the oxidation wave of the materials deposited as thin films on the surface of the working electrode. LUMO energy level (E_{LUMO}) was estimated by adding the optical bandgap (E_g) to the corresponding HOMO energy level as in **Equation S16**:
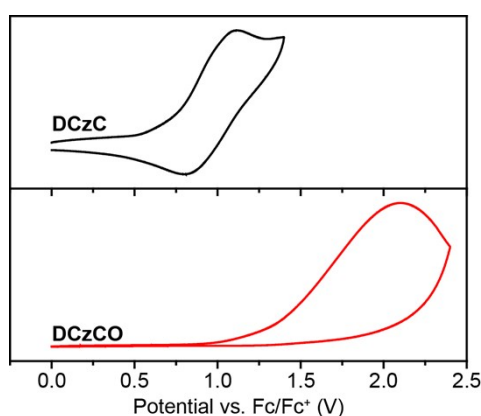
$$E_{LUMO} = E_{HOMO} + E_g \qquad (S16)$$

Figure S15. Cyclic voltammograms of **DCzC** and **DCzCO**.

Table S7. Photophysical and electrochemical properties of **DCzC** and **DCzCO**.

Compd.	T_d/T_g (°C)	λ_{abs} (nm)		$E_g{}^a$ (eV)	λ_{em} (nm)		$E_T{}^b$ (eV)	PLQY (%)	τ (ns)	CV (eV)	
		CH$_2$Cl$_2$	Film		CH$_2$Cl$_2$	Film				HOMO	LUMO^e
DCzC	297/111	292, 322, 335	302, 334, 348	3.59	341, 357	365, 403	3.02	20.5^c/85.03^d	1.5, 10.9	-5.47	-1.88
DCzCO	257/-	289, 303, 315	292, 306, 318	3.84	339, 354	342, 430	3.01	5.4^c/94.39^d	4.0, 3.7	-6.07	-2.23

[a]Optical band gap (E_g) calculated by the absorption edge technique in CH$_2$Cl$_2$; [b]Triplet energy (E_T) obtained from phosphorescent spectrum; [c]Photoluminescence quantum yield (PLQY) in pure film; [d]Photoluminescence quantum yield (PLQY) of the FIrpic-doped film; [e]LUMO energy level estimated by adding E_g to the HOMO energy level.

Table S8. ωB97x calculated reorganization energies (λ_h for hole, λ_e for electron) of **DCzC** and **DCzCO** (in eV).

Compound	λ_h (eV)	λ_e (eV)
DCzC	0.335	0.184
DCzCO	0.667	0.692

8. Devices fabrication and measurements

Single carrier transporting device. The charge transport properties were experimentally investigated by single-carrier charge transporting devices, under the devices structures of ITO/ poly(3,4-ethylenedioxythiophene): poly(styrenesulfonate) (PEDOT:PSS) (30 nm)/ 1,3,5-triazo-2,4,6-triphosphorine- 2,2,4,4,6,6-tetrachloride (TAPC) (20 nm)/ N, N'-dicarbazolyl-3,5-benzene (mCP) (8 nm)/ host (20 nm)/ mCP (8 nm)/ TAPC (20 nm)/ molybdenum trioxide (MoO$_3$) (10 nm)/ Al for hole only device and ITO/ lithium fluoride (LiF) (1 nm)/ 1,3,5-tri(m-pyrid-3-yl-phenyl) benzene (TmPyPB) (30 nm)/ host (20 nm)/ TmPyPB (30 nm)/ LiF (1 nm)/Al for electron-only device, respectively.

Organic light emitting diode (OLED) devices. Both blue phosphorescent OLED (PhOLEDs) and thermally activated delayed fluorescence (TADF) OLEDs using **DCzC** and **DCzCO** as host materials were investigated. The electroluminescent devices were fabricated with the configurations of ITO/ PEDOT: PSS (30 nm)/ TAPC (20 nm)/ mCP (8 nm)/ host: 18 wt% iridium(III) [bis(4,6-difluorophenyl)- pyridinato-N,C2'] picolinate (FIrpic) (20 nm)/ TmPyPB (30 nm)/ LiF (1 nm)/ Al (100 nm) for blue PhOLEDs and ITO/ PEDOT: PSS (30

nm)/ TAPC (20 nm)/ *m*CP (8 nm)/ host: 30 wt% bis-[4-(9,9-dimethyl-9,10-dihydroacridine)-phenyl]-sulfone (DMAC-DPS) (20 nm)/ diphenylphosphine oxide-4-(triphenylsilyl)phenyl (TSPO1) (5 nm)/ 1,3,5-tris(*N*-phenylbenzimidazol-2-yl)benzene (TPBi) (35 nm)/ LiF (1 nm)/ Al (100 nm) for blue TADF OLEDs, respectively. In these devices, FIrpic and DMAC-DPS were selected as the blue phosphorescent dopant and TADF emitter, respectively; *m*CP and TSPO1 act as the exciton-blocking layer; TAPC, TmPyPB and TPBi function as the hole-transporting layer (HTL) and electron-transporting layer (ETL), respectively; PEDOT: PSS and LiF were used as hole- and electron-injecting layers, respectively.

In a general procedure, ITO-coated glass substrates were etched, patterned, and washed with detergent, deionized water, acetone, and ethanol in turn. After ultraviolet (UV)-ozone treating for 4 min, PEDOT: PSS (30 nm) was spin coated on the ITO substrate and dried at 120ºC in a vacuum oven for 15 min. The other organic layers were deposited by thermal evaporation under a pressure of 4×10^{-4} Pa in a rate of 0.1-0.2 nm s^{-1}. The layer thickness and the deposition rate were monitored *in situ* by oscillating quartz thickness monitors. The devices without encapsulation were measured immediately after fabrication under ambient atmosphere at room temperature. Electroluminescent (EL) spectra of the devices were measured by a PR655 spectra scan spectrometer. The luminance-voltage and current–voltage characteristics were recorded using an optical power meter and a Keithley 2602 voltage current source. And the external quantum efficiency (EQE) was calculated according to **Equation S17**.

$$EQE = \frac{\pi e \eta_{cd/A} \int \lambda p(\lambda) d\lambda}{hcK_m \int p(\lambda) \Phi(\lambda) d\lambda} \tag{S17}$$

where $\eta_{cd/A}$ is the current efficiency (cd/A); h is the Planck constant; c is the speed of light in vacuum; λ is the wavelength (nm); e is the electron charge; $p(\lambda)$ is relative electroluminescent intensity at each wavelength; $\Phi(\lambda)$ is the Commission International del'Eclairage chromaticity (CIE) standard photopic luminous efficiency function; and K_m is a constant of 683 lm/W.
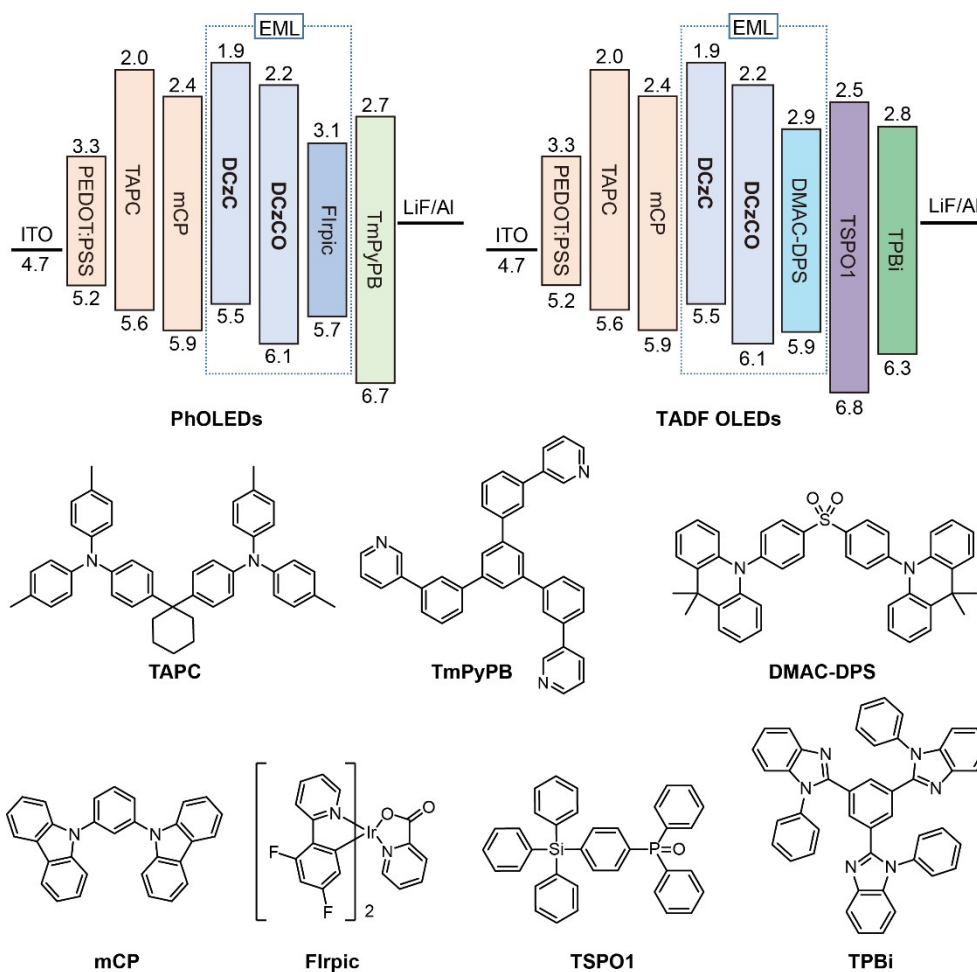
Figure S16. Device configuration of the PhOLEDs and TADF OLEDs hosted by **DCzC** and **DCzCO** with molecular structures of the related materials used in these devices. The configuration of PhOLED is ITO/PEDOT: PSS (30 nm)/ TAPC (20 nm)/ mCP (8 nm)/ host: 18 wt% FIrpic (20 nm)/ TmPyPB (30 nm)/ LiF (1 nm)/ Al (100 nm), while that of TADF OLED is ITO/ PEDOT: PSS (30 nm)/ TAPC (20 nm)/ mCP (8 nm)/ host: 30 wt% DMAC-DPS (20 nm)/ TSPO1 (5 nm)/ TPBi (35 nm)/ LiF (1 nm)/ Al (100 nm).
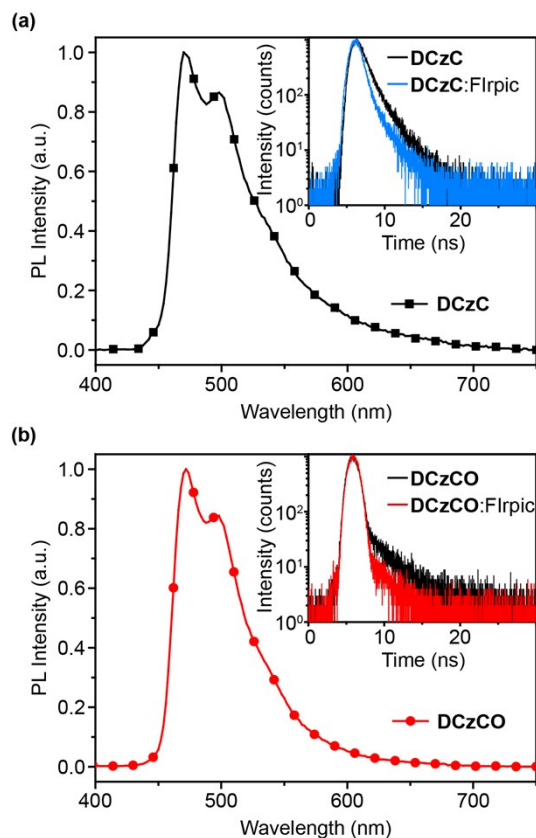
Figure S17. Photoluminescent (PL) spectra of FIrpic-doped (18 wt%) (a) **DCzC** and (b) **DCzCO** films and transient PL decay curves (inset) of the host emission at 365 and 345 nm with or without 18 wt% FIrpic doping. The excitation wavelength is at 295 nm.
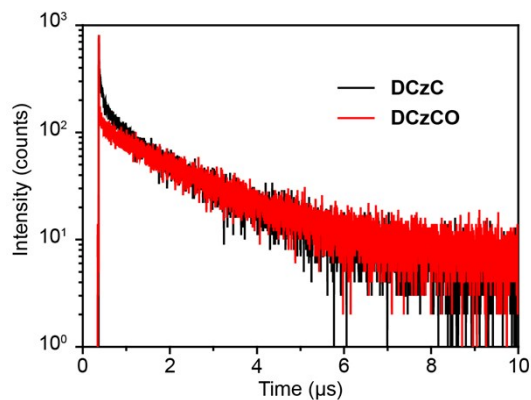

Figure S18. Transient PL decay curves (478 nm) of FIrpic-doped (18 wt%) (a) **DCzC** and (b) **DCzCO** films. The excitation wavelength is 295 nm.

Table S9. A brief summary of the reported device performance of the FIrpic-based PhOLEDs using single host material.

Host	V_{on} (V)[a]	EQE (%)[b]	CE (cd/A)[b]	PE (lm/W)[b]	CIE (x, y)	Ref.
SitCz	2.9	27.2	46.3	36.5	(0.13, 0.29)	7
2,6DCZPPY	3.2	27.3	53.95	51.9	(0.14, 0.32)	8
DCPPO	3.5	27.5	53.0	42.7	(0.15, 0.32)	9
TCbzBz	3.0	28.0	58.2	59.4	-	10
CbOTCb	~3.5	28.7	47.4	44.0	(0.14, 0.30)	11
m-DCz-S	2.8	29.0	65.2	69.7	-	12
PCb-PCz	~3.4	29.6	-	44.2	(0.14, 0.28)	13
CbBPCb	~3.5	30.1	53.6	50.6	-	14
mCPCN	~3.1	30.6	73.4	67.8	(0.16, 0.36)	15
4-CbzBiz	4.0	30.9	64.1	66.3	-	16
PCPO25	3.0	31.4	-	53.1	-	17
DCzC	4.0	7.2	14.7	11.3	-	This work
DCzCO	3.5	31.2	63.7	53.3	-	This work

[a]V_{on}, turn-on voltage at 1 cd m^{-2}; [b]Maximum efficiency.
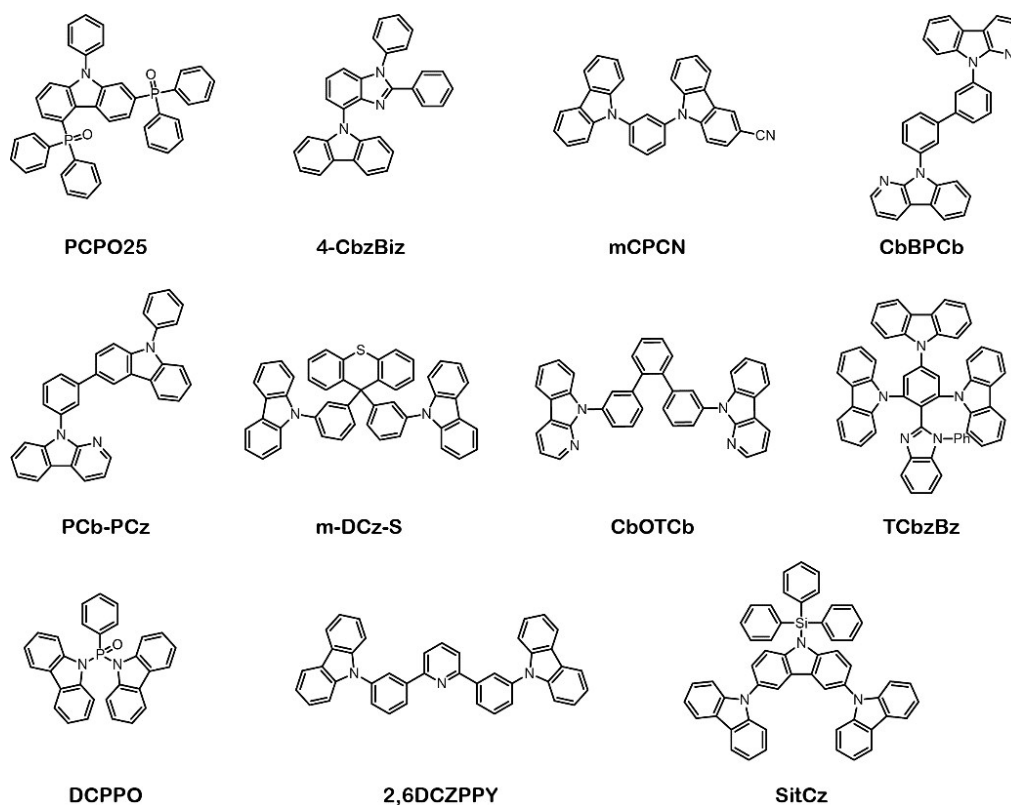
Scheme S3. Molecular structures of the host materials used in the high-performance FIrpic-based PhOLEDs listed in **Table S9**

References:

[1]   Y. Cheng, S. Yang, C. Hsu, *Chem. Rev.* **2009**, *109*, 5868.

[2]   J. Bergman, R. Carlsson, B. Sjoberg, J. Y. Lee, *J. Heterocyclic. Chem.* **1977**, *14*, 1123.

[3]   M. J. Frisch, G. W. Trucks, H. B. Schlegel, G. E. Scuseria, M. A. Robb, J. R. Cheeseman, G. Scalmani, V. Barone, G. A. Petersson, H. Nakatsuji, X. Li, M. Caricato, A. Marenich, J. Bloino, B. G. Janesko, R. Gomperts, B. Mennucci, H. P. Hratchian, J. V. Ortiz, A. F. Izmaylov, J. L. Sonnenberg, D. Williams-Young, F. Ding, F. Lipparini, F. Egidi, J. Goings, B. Peng, A. Petrone, T. Henderson, D. Ranasinghe, V. G. Zakrzewski, J. Gao, N. Rega, G. Zheng, W. Liang, M. Hada, M. Ehara, K. Toyota, R. Fukuda, J. Hasegawa, M. Ishida, T. Nakajima, Y. Honda, O. Kitao, H. Nakai, T. Vreven, K. Throssell, J. A. Jr. Montgomery, J. E. Peralta, F. Ogliaro, M. Bearpark, J. J. Heyd, E. Brothers, K. N. Kudin, V. N. Staroverov, T. Keith, R. Kobayashi, J. Normand, K. Raghavachari, A. Rendell, J. C. Burant, S. S. Iyengar, J. Tomasi, M. Cossi, J. M. Millam, M. Klene, C. Adamo, R. Cammi, J. W. Ochterski, R. L. Martin, K. Morokuma, O. Farkas, J. B. Foresman, D. J. Fox, *Gaussian 09*, Inc.: Wallingford **2016**, Revision E.01, Gaussian, CT.

[4]   I. C. Anjos, M. L. A. A. Vasconcellos, G. B. Rocha, *Theor. Chem. Acc.* **2012**, *131*, 1294.

[5]   T. Lu, F. Chen, *J. Comput. Chem.* **2012**, *33*, 580.

[6]   Y. Tao, L. Xu, Z. Zhang, R. Chen, H. Li, H. Xu, C. Zheng, W. Huang, *J. Am. Chem. Soc.* **2016**, *138*, 9655.

[7]   J. Bin, N. Cho, J. Hong, *Adv. Mater.* **2012**, *24*, 2911.

[8]   J. Liu, M. Jiang, X. Zhou, C. Zhan, J. Bai, M. Xiong, F. Li, Y. Liu, *Synthetic. Met.* **2017**, *234*, 111.

[9]   Z. Zhao, G. Yu, Q. Chang, X. Liu, Y. Liu, L. Wang, Z. Liu, Z. Bian, W. Liu, C. Huang, *J. Mater. Chem. C* **2017**, *5*, 7344.

[10]   J. Huang, L. Yun, T. Kung, C. Chen, J. Lee, Y. Wu, T. Chiu, P. Chou, M. Leung, *J. Mater. Chem. C* **2017**, *5*, 3600.

[11]   C. W. Lee, Y. Im, J. Seo, J. Y. Lee, *Chem. Commun.* **2013**, *49*, 9860.

[12]   K. Liu, X. Li, M. Liu, D. Chen, X. Cai, Y. Wu, C. Lo, A. Lien, Y. Cao, S. Su, *J. Mater. Chem. C* **2015**, *3*, 9999.

[13]   C. W. Lee, J. Y. Lee, *Chem. Mater.* **2014**, *26*, 1616.

[14]   C. W. Lee, J. Y. Lee, *Adv. Mater.* **2013**, *25*, 5450.

[15]   M. Sarma, W. Tsai, W. Lee, Y. Chi, C. Wu, S. Liu, P. Chou, K. Wong, *Chem* **2017**, *3*, 461.

[16]   S. Chang, G. Lin, Y. Cheng, J. Huang, C. Chang, C. Lin, J. Lee, T. Chiu, M. Leung, *ACS. Appl. Mater. Inter.* **2018**, *10*, 42723.

[17]   M. Kim, J. Y. Lee, *Adv. Funct. Mater.* **2014**, *24*, 4164.